SIAM J. SCI. COMPUT.
Vol. 29, No. 6, pp. 2442–2463

A NUMERICAL BIFURCATION ANALYSIS OF THE ORNSTEIN–ZERNIKE EQUATION WITH HYPERNETTED CHAIN CLOSURE*

R. E. BEARDMORE†, A. T. PEPLOW†, AND F. BRESME‡

Abstract. We study the codimension-one and -two bifurcations of the Ornstein–Zernike equation with hypernetted chain (HNC) closure with Lennard–Jones intermolecular interaction potential. The main purpose of the paper is to present the results of a numerical study undertaken using a suite of algorithms implemented in MATLAB and based on pseudo arc-length continuation for the codimension-one case and a Newton-GMRES method for the codimension-two case. Through careful consideration of the results of our computations, an argument is formulated which shows that *spinodal* isothermal solution branches arising in this model cannot be reproduced numerically. Furthermore, we show that the existence of an upper bound on the density that can be realized on a vapor isothermal solution branch, which must be present at a spinodal, causes the existence of at least one fold bifurcation along that *vapor* branch when density is used as the bifurcation parameter. This provides an explanation for previous inconclusive attempts to compute solutions using Newton–Picard methods that are popular in the physical chemistry literature.

Key words. Ornstein–Zernike equation, spinodal, liquid phase, vapor phase

AMS subject classifications. 47J10, 45G10, 82B26, 82B80

DOI. 10.1137/060650659

Invitation. We invite the interested reader to email author R. E. Beardmore in order to obtain a copy of the MATLAB codes developed for this study.

1. Introduction.

The subject of this paper is the Ornstein–Zernike (OZ) equation that was presented almost a century ago to model the molecular structure of a fluid at varying densities [18]:

$$h(\|\mathbf{x}\|) = c(\|\mathbf{x}\|) + \rho \int_{\mathbb{R}^3} h(\|\mathbf{x}-\mathbf{y}\|)c(\|\mathbf{y}\|)d\mathbf{y}. \tag{1.1}$$

Here, $\mathbf{x}, \mathbf{y} \in \mathbb{R}^3$ are spatial coordinates and due to the assumed isotropy of the fluid we need only the radial coordinate $r = \|\mathbf{x}\|$, where $\|\cdot\|$ is the Euclidean distance function. The parameter ρ is the mean particle density of the fluid at temperature T, where $\beta = 1/(k_B T)$ will be used to denote the Boltzmann factor and $u(r)$ the intermolecular potential, a typical example of which is given below. The total (h) and direct (c) correlation functions yield the indirect correlation function of the fluid, $\gamma = h - c$, and the radial distribution function $g(r) = 1 + h(r)$ is the pair correlation function of molecules in the fluid.

The last two years or so have seen an increased use of continuation algorithms in liquid state theory. This can be seen both in [10, 9] in the context of density functional theory and in a study of the OZ equation [15]. The authors of [10, 9] make the express comment that continuation algorithms are needed to track phase transitions, and the

*Received by the editors January 23, 2006; accepted for publication (in revised form) April 5, 2007; published electronically October 17, 2007.
http://www.siam.org/journals/sisc/29-6/65065.html
†Department of Mathematics, Imperial College, 180 Queen's Gate, South Kensington, London, SW7 2AZ (r.beardmore@ic.ac.uk, atpeplow@kth.se).
‡Department of Chemistry, Imperial College, Exhibition Road, South Kensington, London, SW7 2AZ (f.bresme@ic.ac.uk).

purpose of this paper is to analyze the correspondence between the solutions of the OZ equation and its discretization using continuation algorithms. In particular, we show that for the OZ equation with *hypernetted chain closure*, a term that is defined below, there is no finite-dimensional projection of the equations and hence no algorithm that can approximate physically meaningful solutions when seeking a *spinodal*, a precursor to a phase transition.

1.1. Closures. In order to form a well-posed mathematical system of equations from (1.1) that can be solved, at least in principle, we impose a closure relationship. This is an algebraic equation or pointwise constraint that augments (1.1) and which is deemed to hold throughout the fluid.

Some closures are structured so that the total correlation function is a perturbation of the *Mayer f-function* that is defined by $f(r) = -1 + e^{-\beta u(r)}$. These closures are obtained beginning with the observation that there is a function $B(r)$ such that

$$h = -1 + e^{-\beta u + h - c + B} \tag{1.2}$$

holds throughout the fluid; B is called the Bridge function [6].

Due to the fact that the potential u will have singularities that may prevent $-\beta u + h - c$ from being well defined, let us rewrite (1.2) in the form $h = -1 + e^{-\beta u} + e^{-\beta u}\left(-1 + e^{h-c+B}\right)$. The hypernetted chain (HNC) closure that interests us dates from the late 1950's (see [23]) and is obtained by setting $B(r)$ to zero, something that is not possible to justify on physical grounds in any generality. Thus, the OZ equation with HNC closure (OZ-HNC) is (1.1) coupled to

$$h = f + e^{-\beta u} \cdot (-1 + e^{h-c}). \tag{1.3}$$

Such an approximation suffers from *thermodynamic inconsistency*, the property that different routes to computing thermodynamic quantities such as compressibility and pressure yield different results. This is often seen as a fundamental flaw of theories based on closures like HNC.

Another often-studied problem in the physical chemistry literature (again see [6] for background and further references) is the OZ equation with Percus–Yevick (PY) closure [19]. This also dates from the 1950's and is obtained by setting $B = \ln(\gamma + 1) - \ln\gamma$, leading to the PY closure

$$h = f + e^{-\beta u} \cdot (h - c). \tag{1.4}$$

We do not study this particular thermodynamically inconsistent form here. These and other closures have been in use for around thirty years, as explained in the review [6], and combinations of different closures have also been proposed, some of which are reviewed in the latter reference, but we have chosen to concentrate on OZ-HNC.

The HNC and PY closures can be written in a general form involving the potential, temperature, and the indirect correlation function through a nonlinearity G, say, as follows:

$$h = f + e^{-\beta u} G(h - c), \qquad G(0) = 0. \tag{1.5}$$

The suite of algorithms we have developed are able to solve (1.1) and (1.5) for any function G with β and ρ as bifurcation parameters. Moreover, solution branches obtained by varying ρ but holding β fixed are called *isotherms*; those obtained by fixing ρ but varying β are *isochores*.

1.2. Local existence. Note that the OZ equation with closure of the form (1.5) can be written as a single integral equation

$$\gamma = \rho(f + e^{-\beta u}G(\gamma)) * (f + e^{-\beta u}G(\gamma) - \gamma), \tag{1.6}$$

and in the remainder we shall use $N_\beta(\gamma)$ to denote the operator formed by the right-hand side of (1.6), so that this integral equation can be written $\gamma = \rho N_\beta(\gamma)$ for brevity.

The following basic existence theorem for (1.6) can be easily proven using the implicit function theorem, but we state it here without proof.

THEOREM 1. *If $G(\gamma) = -1 + e^\gamma, \beta > 0$, and $f \in L^1(\mathbb{R}^3), \cap L^\infty(\mathbb{R}^3)$, then there is a $\rho' > 0$ such that (1.6) has a solution $\gamma \in L^1(\mathbb{R}^3) \cap L^\infty(\mathbb{R}^3)$ for each $0 \le \rho < \rho'$.*

As a result, one generally requires the short-range condition that f is integrable and bounded over $\mathbb{R}^3$ for $\beta > 0$, a property that follows from the assumption that $\int_1^\infty r^2 u(r)dr < \infty$ such that u is measurable on $(0, \infty)$ and continuous on a half-neighborhood of zero and $\lim_{r\to 0_+} u(r) = +\infty$.

Our algorithms are implemented with the assumption that u is smooth on $(0, \infty)$; we do not perform any computations where the potential is nonsmooth, although it is common in the literature to do so [6, 13, 16]. Indeed, all computations presented here use the Lennard–Jones (LJ) 6-12 potential,

$$u_{LJ}(r) = 4\epsilon\left(\left(\frac{\sigma}{r}\right)^{12} - \left(\frac{\sigma}{r}\right)^{6}\right),$$

where σ is particle diameter and ϵ controls the well-depth. In accordance with [12], we shall express thermodynamic quantities such as density and temperature in reduced units, $\rho^* = \rho\sigma^3$, $T^* = k_B T/\epsilon = 1/(\epsilon\beta)$, although $\sigma = \epsilon = 1$ hold throughout the paper so that $\rho = \rho^*$ and $T^* = 1/\beta$.

1.3. Spinodals. Let us define the *inverse isothermal compressibility* of a fluid

$$\chi^{-1}(c, \rho) := 1 - \rho \int_{\mathbb{R}^3} c(\|\mathbf{x}\|)d\mathbf{x}. \tag{1.7}$$

This quantity plays a fundamental role in the solution of (1.1) and (1.5) for the following reason.

DEFINITION 1. *Let $\beta > 0$ be fixed. A spinodal is said to occur in the OZ-HNC equation (1.1) and (1.5) at $\rho = \rho_{sp}$ if there is a sequence (h_n, c_n, ρ_n) of solutions such that $\rho_n \to \rho_{sp}$ as $n \to \infty$ and $\chi^{-1}(c_n, \rho_n) \to 0$.*

As the temperature is reduced the separation of two phases in the fluid, one liquid and one vapor, begins with the creation of two spinodals at a critical value of temperature and density, T_c and ρ_c. Thus the search for two thermodynamic phases begins with the search for a codimension-two point at which a single critical solution can be found, with $T = T_c$ and $\rho = \rho_c$, say, at which inverse isothermal compressibility is zero.

One consequence of the existence of two spinodals that lie on vapor and liquid isotherms is a region of densities between the two where no solution of (1.6) exists; this region is sometimes called a *no-solution region*. Several analyses based on numerical solutions of the discretized OZ equations appear to have established that a *no-solution region* exists [24, 3, 2, 17, 22], and the purpose of this paper is to investigate these claims further, noting that *none* of the cited references use bifurcation algorithms in their studies. Note in particular [20, Fig. 4] whereby a conjectured series of solution

branches have been drawn; we shall demonstrate that this figure is essentially correct but that there may well be more fold bifurcations present than are shown in [20].

Although we shall show that we are not strictly able to locate phase transitions by applying continuation algorithms to (1.6), we shall use the following suggestive terminology. Isotherms that contain the low-density base solution of (1.6) given by $h = f, c = f$, and $\rho = 0$ will be called *vapor* branches throughout. If there are two isothermal solution branches, the one associated with higher densities will be called the *liquid* branch. We shall also use the prefix *discrete* to denote that these terms apply to solution branches of a discretization of (1.6).

1.3.1. Fold bifurcations and pseudospinodals. Let us consider for a moment the following definition of fold bifurcation, noting that it also incorporates solution branches that intersect in pitchfork or transcritical bifurcations.

DEFINITION 2 (fold bifurcation). *Let X be a Banach space. The nonlinear equation $F(\gamma, \rho) = 0$, where $F : X \times \mathbb{R} \to X$, is said to possess a fold bifurcation at ρ_{FB} if there is a $\gamma_{FB} \in X$ and at least two distinct sequences $(\gamma_n) \in X$ and $(\overline{\gamma}_n) \in X$ such that for some sequence $(\rho_n) \subset \mathbb{R}$*

(i) *$F(\gamma_n, \rho_n) = 0$ and $F(\overline{\gamma}_n, \rho_n) = 0$ for all n,*
(ii) *$\rho_n < \rho_{FB}$ for all n, and*
(iii) *$\lim_{n\to\infty}(\gamma_n, \rho_n) = \lim_{n\to\infty}(\overline{\gamma}_n, \rho_n) = (\gamma_{FB}, \rho_{FB}) \in X \times \mathbb{R}$.*

The reason for introducing this definition is that while phase transitions begin with a search for spinodals, it was noted as long ago as 1968 for the PY closure [1] (see [1, Fig. 1] in particular) that fold bifurcations could occur where one might anticipate the existence of spinodals. As a result, fold bifurcations in the context of (1.6) are often called *pseudospinodals*, although *square-root branch points* [2] are also used. Let us again remark that Definition 2 encompasses a greater class of solution curves than simply those with the typical folded structure at a bifurcation point, but the theorems later in the paper are only able to demonstrate the existence of a fold bifurcation in the sense of Definition 2.

Using a standard codimension-one formulation of (1.6), we shall compute curves that illustrate how fold bifurcations of (1.6) vary as a function of temperature and density, and these rather resemble *phase diagrams* and may be thought of as *an approximation* of the boundary of the region of liquid-vapor coexistence.

The basic Newton method has been seen as the most appropriate algorithm for studying (1.6), which is why continuation algorithms were not used to study the OZ equation until very recently [15]. Moreover, the various codimension-two problems associated with OZ have yet to be tackled directly in the physical chemistry literature; hence this paper addresses these issues. This is perhaps a little surprising given the debate that took place in [11, 5, 4, 7] regarding the errors committed when employing inappropriate numerical techniques. Moreover, the study of the correspondence between analytical and numerical solutions of the OZ equation with PY closure performed in [7] shows surprising discrepancies that, to the best of the authors' knowledge, have not received adequate attention in the literature.

Typical behavior: Unphysical isotherms part I. In anticipation of the results to follow, in Figure 1.1 we have plotted a locus of fold bifurcations for (1.6) that has been computed for an LJ fluid using a codimension-one formulation of the OZ-HNC equation; note its resemblance to a phase diagram. (The meaning of the parameter $R = 10\sigma$ that appears in the caption of this figure is explained later in the paper.)

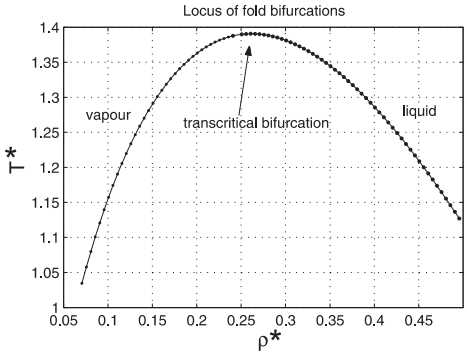

FIG. 1.1. *(LJ potential, HNC closure, $R = 10\sigma$ with $2^{12} + 1$ mesh points.) A locus of fold bifurcations showing liquid and vapor branches created at a transcritical bifurcation. Below the parabolic curve there are regions where no solution exists bounded by two fold bifurcations that occur as ρ is varied and β is fixed; one occurs on the liquid branch and one occurs on the vapor branch (see Figure* 1.2*).*

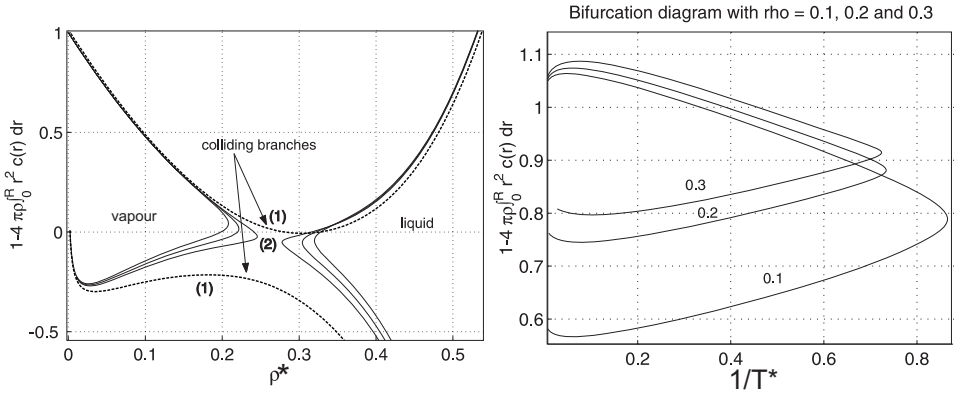

FIG. 1.2. *(LJ potential, HNC closure, $R = 10\sigma$, $2^{12} + 1$ mesh points.) (Left) Two supercritical branches (at* (1)*) touch (near* (2)*) and exchange singularities: Inverse compressibility plotted against density with label* (1) $\beta = 0.696$*, label* (2) $\beta = 0.72$*; two more liquid-vapor isothermal pairs are shown with lower temperatures at* $\beta = 0.725$ *and* 0.73*. (Right) Three isochores showing fold bifurcations at low temperatures; density is fixed at* $\rho = 0.1, 0.2, 0.3$*.*

In Figure 1.2 (left) we have computed a set of isothermal solution branches that show density plotted on the horizontal axis against inverse isothermal compressibility on the vertical axis; to produce each curve, temperature is lowered and a pair of computations is performed, and the resulting figure is an *unfolding* of the apex from Figure 1.1. Label (2) in Figure 1.2 (left) sees the creation of two fold bifurcations or *pseudospinodals* that arise due to a collision of two solution branches, one of which is a vapor branch with positive compressibility, but the other has negative compressibility and is therefore not a branch of physically meaningful solutions.

1.4. Notation. Given a nonlinear mapping $N(\gamma)$ on a Banach space X that contains elements γ and h, $dN(\gamma)[h]$ denotes the Fréchet derivative and $BL(X)$ is the space of bounded, linear mappings from X to itself. We shall write $N_\beta(\gamma)$ to emphasize the dependence of N on a parameter β, but we shall suppress the subscript otherwise. The dual space of all bounded linear functionals on X is written X^*.

Numerical objects that correspond to infinite-dimensional objects will be written using a bold font, so that $\boldsymbol{\gamma}$ will be a vector that corresponds to a correlation function γ projected onto a finite-dimensional subspace of X. The set $\{\mathbf{e}_j\}_{j=0}^n$ is used to denote the standard basis vectors of $\mathbb{R}^{n+1}$. We shall write $B_R(\mathbf{0}) = \{\mathbf{x} \in \mathbb{R}^3 : \|\mathbf{x}\| < R\}$ for a ball in $\mathbb{R}^3$, and $\langle \mathbf{u}, \mathbf{v} \rangle$ is the standard Euclidean inner product of vectors $\mathbf{u}, \mathbf{v} \in \mathbb{R}^{n+1}$.

We depart a little from convention by using $L^p(\mathbb{R}^3)$ to denote the space $\{u : \mathbb{R}^3 \to \mathbb{R} : \int_{\mathbb{R}^3} |u(\mathbf{x})|^p d\mathbf{x} < \infty\}$, where $p \geq 1$, and $C^0(\mathbb{R}^3)$, $C_0^\infty(\mathbb{R}^3)$, and $L^\infty(\mathbb{R}^3)$ are defined analogously (the point is that the range of functions in these spaces is always $\mathbb{R}$). By $C^{\mathrm{Lip}}(\Omega)$ for a domain $\Omega \subset \mathbb{R}^3$ we understand the space $\{u \in C^0(\overline{\Omega}) : \exists K > 0 \text{ s.t. } |u(\mathbf{x}) - u(\mathbf{y})| \leq K\|\mathbf{x} - \mathbf{y}\|\}$ endowed with a standard norm.

We will use a majuscule to represent the Fourier transform of a minuscule, as in

$$\mathcal{F}(c)(\mathbf{s}) := C(\mathbf{s}) = \int_{\mathbb{R}^3} c(\mathbf{x}) e^{i\mathbf{x}\cdot\mathbf{s}} d\mathbf{x}.$$

The convolution of radially symmetric functions can be written using the convolution theorem and the Hankel transform $\mathcal{H}$, the Fourier transform of radially symmetric functions that is given by

$$\mathcal{H}(a)(s) = 4\pi \int_0^\infty \operatorname{sinc}(rs) r^2 a(r) dr$$

so that $\mathcal{H}^{-1}(a)(s) = \frac{1}{2\pi^2} \int_0^\infty \operatorname{sinc}(rs) r^2 a(r) dr$. Thus we may define a convolution operator by $a * b = \mathcal{H}^{-1}((\mathcal{H}a) \cdot (\mathcal{H}b))$, where $a, b : [0, \infty) \to \mathbb{R}$ are given functions.

2. Observations on the OZ-HNC equation. Throughout the remainder of the paper let us consider (1.6) with the HNC closure $G(\gamma) = -1 + e^\gamma$:

$$\gamma = \rho(f + e^{-\beta u(r)}(-1 + e^\gamma)) * (f + e^{-\beta u(r)}(-1 + e^\gamma) - \gamma). \tag{2.1}$$

Formulation (2.1) is advantageous from a theoretical point of view because G can be regarded as a function that maps $L^1(\mathbb{R}^3) \cap L^\infty(\mathbb{R}^3)$ to itself, a property that is not shared by either of the functions $\gamma \mapsto e^\gamma$ or $\gamma \mapsto \gamma - 1$. As this paper is written from a computational perspective, (2.1) will be rewritten in the more common form

$$\gamma = \rho(-1 + e^{-\beta u(r)} e^\gamma) * (-1 + e^{-\beta u(r)} e^\gamma - \gamma).$$

2.1. Spinodals: Bifurcations at infinity in $L^1(\mathbb{R}^3)$. Applying the Fourier transform to (1.1), we obtain the quadratic algebraic equation that holds almost everywhere,

$$H(s)(1 - \rho C(s)) = C(s), \tag{2.2}$$

where $s \in \mathbb{R}$ is the wave number and H and C are the Fourier transforms of h and c, respectively.

LEMMA 2.1. *There is no pair* $(h, c) \in L^1(\mathbb{R}^3) \times L^1(\mathbb{R}^3)$ *that satisfies* (1.1) *and* $\chi^{-1}(c, \rho) = 0$.

Proof. Suppose that a solution (h, c) of (1.1) exists at a given ρ and that $\chi^{-1}(c, \rho) = 0$. Then $1 = \rho C(0) = \rho \int_{\mathbb{R}^3} c d\mathbf{x}$ but (2.2) yields (on allowing $s \to 0$)

$$H(0) \cdot (1 - \rho C(0)) = C(0) \Longrightarrow \int_{\mathbb{R}^3} h d\mathbf{x} \cdot \chi^{-1}(c, \rho) = \int_{\mathbb{R}^3} c d\mathbf{x} = 0,$$

which is a contradiction. ∎

Suppose that an isothermal solution branch of (1.1) and (1.5) exists (call it $\mathcal{C}$) and suppose that it lies in $L^1(\mathbb{R}^3) \times L^1(\mathbb{R}^3) \times \mathbb{R}$. Suppose also that there is a sequence of low-density solutions in $\mathcal{C}$, so that $\mathcal{C}$ connects to the vapor base solution where $\rho = 0$ and therefore $\chi^{-1}(c, \rho)$ is positive along the low-density part of $\mathcal{C}$.

Now suppose that $\mathcal{C}$ contains a *spinodal* in the sense that there is a sequence $(h_n, c_n, \rho_n) \in \mathcal{C}$ such that $\rho_n \to \rho_{sp} > 0$ and $\lim_{n\to\infty} \chi^{-1}(c_n, \rho_n) = 0$. From (2.2) upon setting $s = 0$ we find

$$\int_{\mathbb{R}^3} h_n d\mathbf{x} \cdot \chi^{-1}(c_n, \rho_n) = \int_{\mathbb{R}^3} c_n d\mathbf{x} \to 1/\rho_{sp},$$

and we must conclude that $\int_{\mathbb{R}^3} h_n(\|\mathbf{x}\|)d\mathbf{x} \to \infty$ as $n \to \infty$. Thus, a spinodal is associated with a bifurcation from infinity in $L^1(\mathbb{R}^3)$. Let us record this in a lemma.

LEMMA 2.2. *Suppose that* $(h_n, c_n, \rho) \subset L^1(\mathbb{R}^3) \times L^1(\mathbb{R}^3) \times \mathbb{R}$ *is a spinodal sequence that accumulates at a nonzero density* $\rho = \rho_{sp}$*; then* $\|h_n\|_{L^1(\mathbb{R}^3)} \to \infty$ *as* $n \to \infty$.

Thus, the fact that a spinodal sequence is a bifurcation at infinity in an $L^1(\mathbb{R}^3)$-norm is a property of the OZ equation alone; whether or not a spinodal is actually present depends essentially on the nature of the closure relationship used in (1.5). For example, the following simple lemma shows that the HNC closure leads to the boundedness of h in the $L^2(\mathbb{R}^3)$-norm at a spinodal, provided that the direct correlation function c in (1.1) is well behaved.

LEMMA 2.3. *Suppose that* $u \in L^1(\mathbb{R}^3 \backslash B_\epsilon(\mathbf{0}))$ *for some* $\epsilon > 0$ *and* (h, c) *solves* (1.1) *and* (1.3) *such that* $\|h\|_{L^\infty} \le M$ *and* $\|c\|_{L^1} + \|c\|_\infty \le M$*. Then there is a* $K_M > 0$ *such that*

$$\int_{\mathbb{R}^3} h(\|\mathbf{x}\|)^2 d\mathbf{x} \le \frac{4\pi\epsilon^2 M^2}{3} + \frac{1}{K_M} \int_{\|\mathbf{x}\|\ge\epsilon} (\beta u + c(\|\mathbf{x}\|))d\mathbf{x}. \tag{2.3}$$

Hence $h \in L^p(\mathbb{R}^3)$ *for all* $2 \le p \le \infty$.

Proof. If we define the function $F(x) = \ln(x + 1) - x$ for all $x > -1$, then $F(0) = 0, F'(0) = 0$, and $F''(x) = -1/(x + 1)^2 < 0$ so that F is concave. Clearly, for each $M > 0$ fixed, there is a $K_M > 0$ such that $F(x) \le -K_M x^2$ for all x such that $-1 < x \le M$. Now, if (h, c) solves (1.1) and (1.3), then from (1.3) we deduce

$$K_M \int_{\|\mathbf{x}\|\ge\epsilon} h^2 d\mathbf{x} \le -\int_{\|\mathbf{x}\|\ge\epsilon} F(h)d\mathbf{x} = \int_{\|\mathbf{x}\|\ge\epsilon} (\beta u + c)d\mathbf{x}$$

because $h(\|\mathbf{x}\|) > -1$ if $\|\mathbf{x}\| > \epsilon$ from the HNC closure. Hence,

$$\begin{aligned}\int_{\mathbb{R}^3} h^2 d\mathbf{x} &\le \int_{\|\mathbf{x}\|\le\epsilon} h^2 d\mathbf{x} + \frac{1}{K_M} \int_{\|\mathbf{x}\|\ge\epsilon} (\beta u + c)d\mathbf{x} \\ &\le M^2 \text{meas}\{\mathbf{x} : \|\mathbf{x}\| \le \epsilon\} + \frac{1}{K_M} \int_{\|\mathbf{x}\|\ge\epsilon} (\beta u + c)d\mathbf{x},\end{aligned}$$

and the result follows. ∎

We can now use the bound from Lemma 2.3 to obtain the following result which states that if a spinodal sequence exists and the correlation functions stay uniformly bounded, and the direct correlation function that is known to be integrable is in fact absolutely integrable, then there are functions $h_0 \in L^2(\mathbb{R}^3) \backslash L^1(\mathbb{R}^3)$ and c_0 that

together satisfy the OZ equation. Any function $h_0 \in L^\infty(\mathbb{R}^3)$ that satisfies an almost-everywhere bound of the form

$$\frac{C}{r^3} < |h_0(\mathbf{x})| < \frac{C'}{r^{(3+\delta)/2}} \qquad \text{(a.a. r} \geq \text{R)}$$

for constants C, C', and R, where $\delta \in (0,3)$ is arbitrary and $r = \|\mathbf{x}\|_2$, the Euclidean length of $\mathbf{x}$, satisfies $h_0 \in L^2(\mathbb{R}^3)\backslash L^1(\mathbb{R}^3)$, and this may give us some clue as to how the total correlation function behaves at a spinodal.

LEMMA 2.4. *Suppose that ρ_{sp} is a density associated with a spinodal sequence $(h_n, c_n, \rho_n) \in L^1(\mathbb{R}^3) \times L^1(\mathbb{R}^3) \times \mathbb{R}$ for $n \geq 1$ and there is an $M > 0$ such that $\|h_n\|_{L^\infty} \leq M$ and $\|c_n\|_{L^1} + \|c_n\|_{L^\infty} \leq M$. Then there are functions $h_0 \in L^2(\mathbb{R}^3)\backslash L^1(\mathbb{R}^3)$ and $c_0 \in L^2(\mathbb{R}^3) \cap L^\infty(\mathbb{R}^3)$ such that*

$$h_0 = c_0 + \rho_{sp}(h_0 * c_0) \quad \text{and} \quad \chi^{-1}(c_0, \rho_{sp}) = 0.$$

Proof. (In this proof, although all functions are defined on $\mathbb{R}^3$, we assume them to be radially symmetric.) The result follows from the continuity of the convolution operator $*$ with respect to weak convergence. For if (h_n, c_n, ρ_n) has the stated properties, then, although $\|h_n\|_{L^1(\mathbb{R}^3)} \to \infty$ as $n \to \infty$, there are bounds of the form

$$\|h_n\|_{L^\infty} \leq M \quad \text{and} \quad \|c_n\|_{L^1} + \|c_n\|_{L^\infty} \leq M$$

that come from the definition of an admissible spinodal sequence. From Lemma 2.3 we may assume that $\|h_n\|_{L^2} \leq M$. We can now apply the Banach–Alaoglu theorem to extract weak and weak* convergent subsequences to find an $h_0 \in L^2$ and a $c_0 \in L^\infty \cap L^2$ such that

$$h_n \rightharpoonup h_0 \text{ in } L^2, c_n \rightharpoonup c_0 \text{ in } L^2, \text{ and } c_n \overset{*}{\rightharpoonup} c_0 \text{ in } L^\infty$$

as $n \to \infty$, using $(L^1)^* \cong L^\infty$ and the fact that $(c_n) \subset (L^1)^*$, which is a bounded sequence.

Now suppose that $\phi \in C_0^\infty(\mathbb{R}^3)$ has support on some closed ball Ω and let $\epsilon > 0$. From the symmetry properties of convolution there is an N_0 such that

$$\begin{aligned}
|\langle \phi, h * c\rangle - \langle \phi, h_n * c_n\rangle| &= |\langle h * \phi, c - c_n\rangle - \langle (h_n - h) * \phi, c_n\rangle| \\
&= |\langle h * \phi, c - c_n\rangle - \langle (h_n - h) * \phi, c_n - c\rangle - \langle (h_n - h) * \phi, c\rangle| \\
&\leq \epsilon + |\langle (h_n - h) * \phi, c_n - c\rangle| + \epsilon
\end{aligned}$$

for all $n \geq N_0$.

Suppose now that $u_n := h_n - h_0 \rightharpoonup 0$ in L^2 and $v_n := c_n - c_0 \rightharpoonup 0$ in L^2 as $n \to \infty$; then $u_n * \phi$ has support in $2 \cdot \Omega$, where $2 \cdot \Omega = \{2\mathbf{x} : \mathbf{x} \in \Omega\}$. Moreover, from the Cauchy–Schwarz inequality

$$\text{ess sup}_{\mathbf{x} \in 2\cdot\Omega} |(u_n * \phi)(\mathbf{x})| \leq \|u_n\|_{L^2} \|\phi\|_{L^2} < \infty$$

and

$$|(u_n * \phi)(\mathbf{x}_1) - (u_n * \phi)(\mathbf{x}_2)| \leq \text{meas}(2 \cdot \Omega)^{1/2} \|\phi\|_{C^1} \|\mathbf{x}_1 - \mathbf{x}_2\| \|u_n\|_{L^2},$$

and we may assume that $u_n * \phi$ is continuous and uniformly bounded. Clearly the Lipschitz norm $\|u_n * \phi\|_{C^{\text{Lip}}(2\cdot\Omega)}$ is bounded and because the embedding $C^{\text{Lip}}(2 \cdot \Omega) \subset$

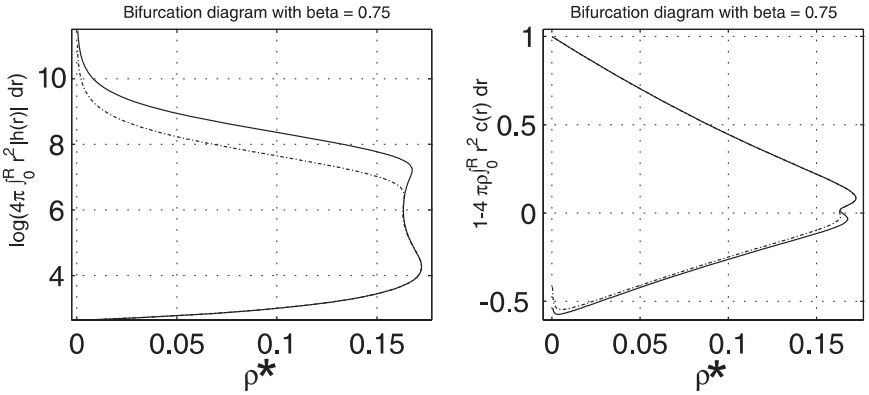

FIG. 2.1. *(LJ potential, HNC closure,* $2^{12}+1$ *mesh points, and* $\beta = 0.75$*.) Two computations with different cut-off parameters* $R = 50\sigma$ *(dashed line) and* 80σ *(full line). Spinodal-like behavior is clearly visible, and note the presence of multiple fold bifurcations.*

$C^0(2\cdot\Omega)$ is compact and $u_n \rightharpoonup 0$ in L^2, it follows that $u_n * \phi \rightharpoonup 0$ in L^2, and so we may assume that $u_n * \phi \to 0$ uniformly on $2\cdot\Omega$.

Hence $|\langle u_n * \phi, v_n\rangle| \leq \|u_n * \phi\|_{C^0(2\cdot\Omega)}\|v_n\|_{L^2}$ and on setting $u_n := h_n - h_0$, $v_n := c_n - c_0$ we have shown that $h_n * v_n \rightharpoonup h_0 * v_0$ in L^2 because $C_0^\infty(\mathbb{R}^3)$ is dense in $L^2(\mathbb{R}^3)$. Since $-h_n + c_n + \rho_n h_n * v_n = 0$ for all n we find that the pair (h_0, c_0) satisfies the OZ equation.

To obtain the zero inverse compressibility of this pair, because $\chi^{-1}(c_n, \rho_n) = 1 - \rho_n \int_{\mathbb{R}^3} c_n(\|\mathbf{x}\|)d\mathbf{x} \to 0$ it suffices to show that $\int_{\mathbb{R}^3} c_n d\mathbf{x} \to \int_{\mathbb{R}^3} c_0 d\mathbf{x}$, which itself follows if $\int_{\mathbb{R}^3} c_n\phi d\mathbf{x} \to \int_{\mathbb{R}^3} c_0\phi d\mathbf{x}$ for all $\phi \in L^\infty$. Now, $c_n \in L^1(\mathbb{R}^3)$ can be viewed as a continuous linear functional in $(L^\infty)^*$ acting via integration, as in $c_n(\psi) = \int_{\mathbb{R}^3} c_n\psi d\mathbf{x}$ and $\|c_n\|_{(L^\infty)^*} \leq \|c_n\|_{L^1}$. The result now follows by applying the Banach–Alaoglu theorem and choosing $\phi = 1$. □

One might call the functions h_0 and c_0 spinodal *semisolutions* because, although they satisfy the OZ equation (1.1), they may well not satisfy the constraint (1.3). Establishing the existence of the a priori bounds needed for Lemma 2.4 depends on the closure (1.5) and is not a straightforward task. However, given that (1.1) is a description of the fluid that holds under any thermodynamic conditions, it is essential that conditions exist such that (1.1) continues to hold whether or not the fluid is at a spinodal.

Computing spinodals: Unphysical isotherms part II. The property of Lemma 2.3 of having a sequence of total correlation functions (h_n) that are $L^2(\mathbb{R}^3)$-bounded but divergent in $L^1(\mathbb{R}^3)$ will cause difficulties for any numerical discretization of (1.1) and (1.5). Indeed, it will force such a discretization to possess uniform a priori bounds because of the equivalence of different norms on finite-dimensional spaces.

This simple observation ensures that admissible spinodal sequences cannot be reproduced easily with a computational procedure, and this may go some way to explaining the claims made in [2, 20] that apparent spinodals in numerically computed solutions are not true spinodals. Moreover, if Lemma 2.3 does provide a description of the fluid through a spinodal, the resulting computations must behave in a manner that produces nonphysical results.

We have illustrated this problem in Figure 2.1 containing two plots. The left-hand figure shows the $L^1(\mathbb{R}^3)$-norm of h plotted on a log scale against density where a very rapid change in this norm takes place over a very small density interval. This is clear

numerical evidence of the existence of a spinodal, and the right-hand plot shows the numerically obtained inverse compressibility χ^{-1} against density, with this variable passing through zero, which seems to confirm this observation. However, yet again we find that there are physically meaningless solutions with negative compressibility.

Clearly, the values of χ^{-1} are very close to zero along the *vertical* part of the branch in the left-hand plot of Figure 2.1. However, a number of fold bifurcations can be seen (three in this plot) and there is a final fold after which the density monotonically decreases before finally heading toward zero as the norm grows further; this is also physically meaningless behavior. We shall give a tentative explanation of this behavior later in the paper and prove that the existence of a spinodal along a vapor branch in a discretization of (1.1) with the HNC closure must yield the existence of a fold bifurcation.

Remark 1. The existence of an apparent solution whereby $\chi^{-1}(c,\rho)=0$ is troublesome in light of Lemma 2.1 and is an artifact of the discretization used to solve (2.1). However, the discretization procedure used to produce Figure 2.1 is standard in the physical chemistry literature: as described in the following section, the fluid is truncated to a ball of radius R, called the cut-off parameter, and (2.1) is solved as an integral equation on the resulting finite domain. In Figure 2.1 we have used two different values for R—one of $R=50\sigma$ and one of $R=80\sigma$, where σ is the particle diameter, here taken to be 1.

3. Computational procedures.

3.1. The cut-off parameter *R*. In all of the liquid-state physics literature that we have cited (see [24, 3, 17, 2, 15], for example), one solves (1.1) numerically by first truncating the region of integration to a finite region, and so we also adopt this procedure. So, rather than solving (1.1), one seeks solutions of a *windowed* integral equation,

$$h(r)=c(r)+\int_{\mathbb{R}^3}[X_{_R}h](\|\mathbf{x}-\mathbf{y}\|)[X_{_R}c](\|\mathbf{y}\|)d\mathbf{y}\qquad(0\le r\le R),\tag{3.1}$$

where $X_{_R}$ is the windowing operator:

$$(X_{_R}v)(\mathbf{x})=\begin{cases} v(\mathbf{x}) & : \quad \|\mathbf{x}\|\le R,\\ 0 & : \quad \text{otherwise.}\end{cases}$$

The region of integration in (3.1) is therefore finite, which permits a straightforward method of discretization to be applied to (3.1) in tandem with the HNC constraint.

Clearly, $X_{_R}$ is a projection operator in the sense that $X_{_R}(X_{_R}(u))=X_{_R}(u)$ for all $u\in L^1(\mathbb{R}^3)$, and so if we set $h_R=X_{_R}h$ and $c_R=X_{_R}c$, (3.1) is equivalent to

$$h_R=c_R+\rho X_{_R}(h_R*c_R),\tag{3.2}$$

so that when we take the Fourier transform of (3.2) we obtain a relationship involving convolution with the transform of the windowing operator applied to the constant function that is identically one, here denoted 1,

$$H_R=C_R+\rho\widehat{X_{_R}(1)}*(H_R\cdot C_R),\tag{3.3}$$

where $\widehat{X_{_R}(1)}(s)=(2R)^{-1/2}s^{-3/2}J_{3/2}(Rs)$ is a certain Bessel function.

The point of this is the Fourier transform of the windowed OZ equation does not lead to an algebraic equation but rather to a convolution equation with a fixed

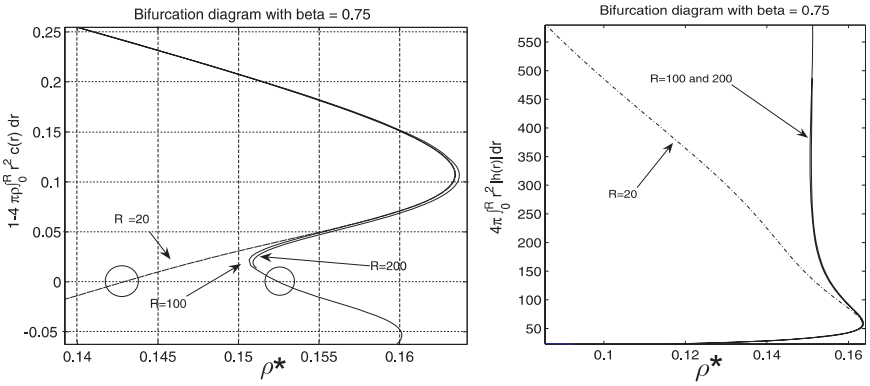

FIG. 3.1. *(LJ potential, HNC closure, $R = 20\sigma, 100\sigma, 200\sigma, \beta = 0.75$, and $2^{13} + 1$ mesh points.) An illustration of the high sensitivity of the bifurcation diagram to changes in the windowing parameter R near an apparent spinodal (marked by circles). (Left) Inverse compressibility against ρ^*. (Right) $L^1(\mathbb{R}^3)$-norm of h against ρ^*.*

kernel, and this makes it difficult to define a *compressibility* functional of the windowed problem (3.1) with the correct qualitative properties. For example, the argument of Lemma 2.1 breaks down when the cut-off procedure is applied, and so the relationship between spinodals and bifurcations from infinity is no longer apparent.

Moreover, if one still defines inverse compressibility in the sense of (1.7), then it may well be possible to realize $L^1(\mathbb{R}^3)$ solutions of the windowed OZ equation (3.1) with zero inverse compressibility. This is illustrated in Figure 3.1 (left), where two regions have been circled that indeed appear to contain numerically computed solutions with zero inverse compressibility.

Based on Figure 3.1 a further comment can be made in terms of the order of convergence of approximate solutions of (3.1) and (1.5) in a suitable norm as $R \to \infty$. One needs estimates of $\|h - X_{_R} h\|_Z$ in some space Z, and, bearing in mind the $L^1(\mathbb{R}^3)$-divergence at a spinodal, the bounds

$$\|h - X_{_R} h\|_Z \leq \begin{cases} 1/(4\pi R^2)\|h - X_{_R} h\|_{L^1(\mathbb{R}^3)} = o(R^{-2}), \\ 1/(4\pi R)^{1/2}\|h - X_{_R} h\|_{L^2(\mathbb{R}^3)} = o(R^{-1/2}) \end{cases}$$

apply with $Z = L^1(0,\infty)$ if $h \in L^1(\mathbb{R}^3) \cap L^2(\mathbb{R}^3)$.

One *may* subsequently anticipate a degradation of the convergence of approximate solutions with respect to R as one nears a spinodal. Indeed, the relatively poor convergence of the bifurcation picture with respect to R is illustrated in Figure 3.1, where a computation is made along an apparent near-spinodal solution branch. Three choices are used, $R = 20\sigma$, 100σ, and 200σ, recalling that the particle diameter σ is 1, where only the larger two of the values resolve a number of bifurcations that seem to be missed when the smaller value is used for R.

3.2. Numerical implementation of OZ-HNC. Suppose that $v : [0,\infty) \to \mathbb{R}$ is a given function, and define the windowed Hankel transforms

$$\mathcal{H}_{_R} v = X_{_R} \mathcal{H}(X_{_R} v) \text{ and } \mathcal{H}_{_R}^{-1} v = X_{_R} \mathcal{H}^{-1}(X_{_R} v);$$

we then finally arrive at the equation that is to be solved as part of our computational study:

$$\gamma = \rho \mathcal{H}_{_R}^{-1}[\mathcal{H}_{_R}(f + e^{-\beta u} G(\gamma)) \cdot \mathcal{H}_{_R}(f + e^{-\beta u} G(\gamma) - \gamma)], \tag{3.4}$$

which is the windowed analogue of (1.6). Now let us briefly explain our discretization of (3.4). First recall that our computations are performed using only the HNC form for G given by $G(\gamma) = -1 + e^{\gamma}$, and note that in the following description, we shall use a subscript applied to a vector in $\mathbb{R}^{n+1}$ to denote a coordinate from that vector.

So, begin by choosing a set of basis functions $\{\phi_i(r)\}_{i=0}^n$ centered on nodes (r_i) of a uniform mesh, taking mesh points $r_i = iR/n$ for $0 \le i \le n$. We seek an approximate solution of (3.4) of the form $\gamma = \sum_{i=0}^n \gamma_i \phi_i(r)$, and the resulting system is projected onto ϕ_j for all $j = 0, \dots, n$. For any such set of basis functions, this procedure yields a finite-dimensional system of equations of dimension $n+1$ and, writing

$$e^{-\beta \mathbf{U}} = (e^{-\beta u(r_i)})_{i=0}^n \text{ such that } (e^{-\beta \mathbf{U}})_0 = 0,$$

$\mathbf{h} = (h_i)_{i=0}^n$, and $\mathbf{c} = (c_i)_{i=0}^n$, the HNC closure yields

$$h_0 = -1,\ h_i = -1 + e^{-\beta u(r_i)} \exp(\gamma_i), \text{ and } c_i = h_i - \gamma_i \qquad (i = 1, \dots, n), \tag{3.5}$$

and we obtain the following system of equations for $\mathbf{h}$ and $\mathbf{c}$:

$$\mathbf{h} = \mathbf{c} + \rho B(\mathbf{h}, \mathbf{c}), \tag{3.6}$$

$$\mathbf{h} = \mathbf{f} + e^{-\beta \mathbf{U}}(-\mathbf{1} + \exp(\mathbf{h} - \mathbf{c})). \tag{3.7}$$

Here $\mathbf{1} = (1, 1, \dots, 1)$ and $B : \mathbb{R}^{n+1} \times \mathbb{R}^{n+1} \to \mathbb{R}^{n+1}$ is a bilinear form that represents a discrete convolution operator and we shall also write, here and throughout,

$$\mathbf{f} = -\mathbf{1} + e^{-\beta \mathbf{U}}$$

for the so-called discrete Mayer f-function.

The convolution operator from (1.1) is the only part of the problem that is discretized in a nontrivial way to give (3.6); the algebraic constraint given by the HNC closure (1.3) simply yields the elementwise constraint (3.7). This means that the bilinear form B in (3.6) is central to any analysis, and we shall assume that B is nonzero and satisfies properties B1–B2 defined as follows:

B1. $B(\mathbf{u}_1 + \mathbf{u}_2, \mathbf{v}) = B(\mathbf{u}_1, \mathbf{v}) + B(\mathbf{u}_2, \mathbf{v})$ and $B(\lambda \mathbf{u}, \mathbf{v}) = \lambda B(\mathbf{u}, \mathbf{v})$,
B2. $B(\mathbf{u}, \mathbf{v}) = B(\mathbf{v}, \mathbf{u})$,
B3. $B(\mathbf{u}, \mathbf{u}) = 0 \Longrightarrow \mathbf{u} = 0$, and
B4. $\langle \mathbf{u}, B(\mathbf{u_1}, \mathbf{u_2}) \rangle = \langle \mathbf{u}_1, B(\mathbf{u}, \mathbf{u_2}) \rangle$
for all $\mathbf{u}_1, \mathbf{u}_2, \mathbf{u}, \mathbf{v} \in \mathbb{R}^{n+1}$, and $\lambda \in \mathbb{R}$.

Properties B1 and B2 are the bilinearity and symmetry properties of convolution, whereas B3 reflects the property of convolution over $\mathbb{R}^d$ whereby if the autocorrelation function is identically zero, that is, if $v * v = 0$, then v is zero almost everywhere. It turns out that B3 is not satisfied by the Hankel transform implemented here and by Kelley and Montgomery–Pettitt [15] for (3.6)–(3.7) because it is based on the sine transform, and a weaker property akin to B3 does hold, but only on a codimension-two subspace of $\mathbb{R}^{n+1}$. Property B4 holds whenever $B(\mathbf{u}, \mathbf{v}) = \varphi F^T(F\mathbf{u} \otimes F\mathbf{v})$ for some constant φ and some linear mapping F, and then B3 holds for such a B if F is invertible, where here and below we use $\otimes$ to denote the elementwise product of two vectors.

The finite-dimensional analogy of (3.4) under the HNC closure is a single equation for $\boldsymbol{\gamma} = (\gamma_i)_{i=0}^n$:

$$\boldsymbol{\gamma} = \rho B(\mathbf{f} + e^{-\beta \mathbf{U}} G(\gamma)), \mathbf{f} + e^{-\beta \mathbf{U}} G(\boldsymbol{\gamma} - \boldsymbol{\gamma}), \tag{3.8}$$

where $G(\boldsymbol{\gamma}) = -1 + \exp(\boldsymbol{\gamma})$. We shall use $\mathbf{N}_\beta(\boldsymbol{\gamma})$ to denote the operator that appears in the right-hand side of (3.8).

For the particular case of piecewise-constant basis functions used to locate approximate solutions of (3.4), we obtain the convolution operator B_n given by

$$B_n(\mathbf{u}, \mathbf{v}) = H^*((H\mathbf{u}) \otimes (H\mathbf{v})) \tag{3.9}$$

and H is a discrete Hankel transform that is defined elementwise by

$$(H\mathbf{u})_j = \left(\frac{R}{n}\right)^3 \frac{4n}{j^2} \sum_{i=1}^{n-1} \left[ij \sin\left(\frac{\pi ij}{n}\right) u_i\right] \qquad (\text{for } 1 \le j \le n-1)$$

and where $(H\mathbf{u})_0 = 2(H\mathbf{u})_1 - (H\mathbf{u})_2$ and $(H\mathbf{u})_n = 2(H\mathbf{u})_{n-1} - (H\mathbf{u})_{n-2}$. Similarly, H^* is the transform defined by

$$(H^*\mathbf{u})_j = \frac{n}{2R^2 j^2} \sum_{i=1}^{n-1} \left[ij \sin\left(\frac{\pi ij}{n}\right) u_i\right] \qquad (\text{for } 1 \le j \le n-1),$$

and this is also extended to the zeroth and nth coordinates by extrapolation. Of course, by the nature of the Hankel transform one can scale H to satisfy $H^2 = I$, but we have not done this; it is, however, clear that there is a constant φ depending on R and n such that $H^* = \varphi H = \varphi H^T$.

3.2.1. Localized vectors. The practical evaluation of the convolution of two vectors via the form B_n can be evaluated using three FFT-sine transforms, and note that the resulting convolution satisfies Properties B1–B2 above: B1 comes from the linearity of H, and B2 is true by definition. However, B3 is *not* satisfied for the following reason:

$$B_n(\mathbf{u}, \mathbf{u}) = \mathbf{0} \Longrightarrow H^*((H\mathbf{u})^2) = \mathbf{0} \Longrightarrow (H\mathbf{u})^2 \in \ker(H^*) = \operatorname{span}\{\mathbf{e}_0, \mathbf{e}_n\},$$

because both H and H^*, when acting on either of the vectors $\mathbf{e}_0 = (1, 0, \ldots, 0)$ or $\mathbf{e}_n = (0, \ldots, 0, 1)$, yield the zero vector.

As a result, $B_n(\mathbf{u}, \mathbf{u}) = \mathbf{0}$ for all $\mathbf{u} \in \operatorname{span}\{\mathbf{e}_0, \mathbf{e}_n\}$, and so we shall call any element of span $\{\mathbf{e}_0, \mathbf{e}_n\}$ a *localized* vector. Note that H is only a pseudoinverse of H^* in the sense that they are mutual inverses only on the space $\{0\} \times \mathbb{R}^{n-1} \times \{0\}$, the orthogonal complement of the space of localized vectors.

3.3. Algorithm implementation. Any smooth system of equations of the form (1.6), (3.4), or (3.8) is amenable to a Picard iteration algorithm for small values of ρ, and so we use this approach to locate a base solution on a solution branch. In the vicinity of a bifurcation, both Picard- and Newton-based iteration methods will fail to converge and one must modify the system to be solved in order to account for this instability. We have therefore adopted the well-known pseudo arc-length (PAL) strategy due to Keller [14] and others: view a solution branch $\mathcal{B}$ as a one-dimensional manifold that can be parameterized by an arc-length parameter s and augment (1.6) with a constraint in order to obtain a well-posed system of equations.

The system we solve in practice, again with a Newton method, is $F(\boldsymbol{\gamma}, \rho, s) = (0, 0)$, where

$$\mathbf{F}(\boldsymbol{\gamma}, \rho, s) \equiv (\boldsymbol{\gamma} - \rho \mathbf{N}_\beta(\boldsymbol{\gamma}), \mathbf{g}(\boldsymbol{\gamma}, \rho, s)), \tag{3.10}$$

and $\mathbf{g}$ is an additional arc-length constraint. In principle, there are many possible choices for the function $\mathbf{g}$, but the constraint used in [14] is

$$\mathbf{g}(\boldsymbol{\gamma}, \rho, s) = \langle \mathbf{s}_0, \boldsymbol{\gamma} - \boldsymbol{\gamma}_0 \rangle + \sigma_0(\rho - \rho_0) - (s - s_0),$$

where $(\mathbf{s}_0, \sigma_0)$ is the unit tangent vector at a given point $(\gamma_0, \rho_0, s_0) \in \mathcal{B}$, so that $\mathbf{F}(\boldsymbol{\gamma}_0, \rho_0, s_0) = 0$.

The difference $ds := s - s_0$ is a fixed and typically small quantity but it is sometimes necessary to reduce ds if $\mathcal{B}$ nears an apparent spinodal as there can be many fold bifurcations over a small interval of densities. We do this by monitoring the number of Newton iterations required to reduce the residual to a prescribed tolerance and reduce ds by a constant factor if this number is four or greater.

The Newton step of the PAL algorithm requires a linear solver, and we use an unpreconditioned, restarted GMRES(20) algorithm. As discussed in [15], this is appropriate for integral equations posed on a finite domain as the nonlinear convolution operator in the right-hand side of (1.6) can be formulated as a compact mapping in a suitable function space, and this leads to robust convergence properties for GMRES without preconditioning.

3.3.1. Computing loci of fold bifurcations. Since the problem (1.1) and (1.5) contains the parameters ρ and β, the location of a fold bifurcation may be considered to vary as a function of either ρ or β. We have therefore implemented an algorithm to compute the locus of bifurcation points as they change with respect to changes in temperature (or, rather, changes in β) by applying a Newton method to a discretization of the following augmented or codimension-two formulation:

$$\boldsymbol{\gamma} = \rho\, \boldsymbol{N}_\beta(\boldsymbol{\gamma}), \tag{3.11}$$

$$\boldsymbol{k} = \rho\, d_{\boldsymbol{\gamma}} \boldsymbol{N}_\beta(\boldsymbol{\gamma})[\boldsymbol{k}], \tag{3.12}$$

$$1 = \frac{1}{n} \sum_{j=0}^{n} \langle \boldsymbol{k}, \mathbf{e}_j \rangle\,. \tag{3.13}$$

Applying a Newton iteration to (3.11)–(3.12) allows us to locate a locus of fold points parameterized by ρ, noting that (3.11)–(3.12) ask that $\boldsymbol{\gamma}$ solve (3.8), but also that the linearization of the system not be invertible due to the existence of a nonzero null vector, $\boldsymbol{k}$, that appears in (3.12). The integral constraint in (3.13) is present only to ensure that $\boldsymbol{k}$ is nonzero.

Again, we used GMRES(20) as the linear solver for the Newton iteration method applied to (3.11)–(3.13). Moreover, because we were able to locate $(\boldsymbol{\gamma}, \boldsymbol{k}, \beta)$ for each candidate ρ in practice, a property that can be seen in Figure 1.1, we had no need to implement the PAL algorithm on (3.11)–(3.13).

3.4. Other details.

3.4.1. A fourth-order convolution operator. In order to increase the order of approximation of the finite-dimensional convolution operator $B_n(\mathbf{u}, \mathbf{v})$ with respect to the mesh parameter n, we utilized a simple Richardson extrapolation scheme that provides a fourth-order convolution form denoted $B_n^4(\mathbf{u}, \mathbf{v})$ that utilizes six FFT-sine operations and a single cubic interpolation.

Analytic derivatives were used for the discretization of (3.10), but these were calculated numerically using B_n rather than B_n^4, although the map $\mathbf{N}_\beta(\boldsymbol{\gamma})$ itself was

calculated using B_n^4. To form the numerical derivative operators of (3.11)–(3.13) we again used a difference formula based on the convolution operator B_n, rather than its fourth-order extension B_n^4. However, to evaluate (3.11)–(3.13) as a nonlinear operator acting on $(\boldsymbol{\gamma}, \boldsymbol{k}, \rho)$, we did use the fourth-order discrete convolution operator B_n^4. Irrespective of the parameter values, we used a high tolerance of 10^{-3} for GMRES, controlling the arc-length ds in such a way that three Newton iterations (or four for some computations) were needed for a nonlinear residual of 10^{-11}.

4. The fundamental property of discrete vapor spinodals. Let us begin this section with a definition.

DEFINITION 3. *A solution branch $\boldsymbol{\mathcal{C}}$ of the discrete OZ equation* (3.8) *(with any closure function G and any bilinear form B) is said to possess a* discrete vapor spinodal *if $(\rho, \boldsymbol{\gamma}) = (0, \mathbf{0}) \in \boldsymbol{\mathcal{C}}$ and $\sup\{\rho : (\rho, \boldsymbol{\gamma}) \in \boldsymbol{\mathcal{C}}\} < \infty$.*

Let us now assume a structure on the function G in (3.8) that is chosen to mimic the behavior of the floating-point realization of the exponential function $-1 + e^{\gamma}$:

G1. $G(\gamma) \geq -1$ and there exists an $m > 0$ such that $G(\gamma) = -1$ for all $\gamma \leq -m$,

G2. G is continuous and monotonic increasing, and it is C^1 smooth on $(-m, +\infty)$, and

G3. G is superlinear in the sense that $\lim_{\gamma \to +\infty} G(\gamma)/\gamma = +\infty$.

Assumption G1 effectively states that e^{-m} is indistinguishable from zero if m is sufficiently large and so is not actually satisfied by the choice $G(\gamma) = -1 + e^{\gamma}$ that yields the HNC closure. However, by taking m to be as large as we like, one can find functions G that satisfy G1–G3 and which are as close as we like to the HNC choice. Given the approximate nature of the integral equation theories considered in this paper, perhaps this is not the unreasonable assumption it first appears to be.

Throughout the remainder of the paper, we shall write g for the inverse of $1 + G$ on the domain $[-m, \infty)$ so that the domain of g is $[0, \infty)$ with range $[-m, \infty)$ and $\lim_{x \to \infty} \mathsf{g}(x)/x = 0$ by G3.

The following proposition shows that the finite-dimensionality of (3.8) ensures that one cannot observe a divergent-in-norm total correlation function independently of the direct correlation function, quite unlike the continuous case.

PROPOSITION 1. *For fixed $\beta > 0$ and any discrete convolution form B that satisfies* B1 *and* B2, *there is a connected set $\mathcal{C} \subset \mathbb{R}^{n+1}$ of solutions of* (3.8) *such that $(\boldsymbol{\gamma}, \rho) = (0, 0) \in \mathcal{C}$ and $\mathcal{C}$ is unbounded in the following sense: for each $M > 0$, a solution pair $(\boldsymbol{\gamma}, \rho) \in \mathcal{C}$ can be found such that $\|\boldsymbol{\gamma}\| + \rho = M$ with $\rho > 0$. As a result, if $\mathcal{C}$ possesses a discrete vapor spinodal, then there is a sequence $(\boldsymbol{\gamma}_k, \rho_k)$ and a $\rho_{\rm sp} \geq 0$ such that $\|\boldsymbol{\gamma}_k\| \to \infty$ and $\rho_k \to \rho_{\rm sp}$ as $k \to \infty$.*

The discrete total and direct correlation functions $\mathbf{h}_k$ and $\mathbf{c}_k$ corresponding to $\boldsymbol{\gamma}_k$ satisfy

$$\mathbf{h} = \mathbf{c} + \rho_k B(\mathbf{h}, \mathbf{c}), \tag{4.1}$$

$$\mathbf{h} = \mathbf{f} + e^{-\beta \mathbf{U}} G(\mathbf{h} - \mathbf{c}). \tag{4.2}$$

If $\|\boldsymbol{h}_k\| \to \infty$, then $\|\boldsymbol{c}_k\| \to \infty$ and $\|\boldsymbol{c}_k\|_\infty \sim \|\boldsymbol{h}_k\|_\infty + o(1)$ as $k \to \infty$.

Finally, suppose B also satisfies B4 *and has the property that $B(\mathbf{e}_0, \mathbf{e}_0) = \mathbf{0}$. Under these additional assumptions if $\|\boldsymbol{c}_k\| \to \infty$, then $\|\boldsymbol{h}_k\| \to \infty$.*

Proof. The existence of $\mathcal{C}$ with the stated properties follows immediately from the implicit function theorem and the Leray–Schauder continuation principle (see [25] for example).

Now suppose that $\mathcal{C}$ is a discrete vapor spinodal; then the only solution of (3.8) with $\rho = 0$ is the base solution $\boldsymbol{\gamma} = \mathbf{0}$, and it follows immediately that any solution pair $(\boldsymbol{\gamma}, \rho) \in \mathcal{C}$ with $\boldsymbol{\gamma} \neq \mathbf{0}$ must satisfy $0 < \rho \leq \rho_{\max}$, where $\rho_{\max} := \sup\{\rho \geq 0 : (\boldsymbol{\gamma}, \rho) \in \mathcal{C}\}$. Hence it follows from the unboundedness of $\mathcal{C}$ in the sense stated that the norm of $\boldsymbol{\gamma}$ must diverge along $\mathcal{C}$.

From (4.2) and G1 it follows that $\mathbf{h} \geq -\mathbf{1}$ and that the zeroth component of $\mathbf{h}$ is $\mathbf{h}_0 = -1$ so that (4.2) can be written

$$\mathsf{g}(e^{\beta \mathbf{U}}(\mathbf{h} + \mathbf{1})) = \mathbf{h} - \mathbf{c}, \tag{4.3}$$

ignoring the undefined zeroth component of $e^{\beta \mathbf{U}}(\mathbf{h}+\mathbf{1})$ *for the moment.* Hence, considering the vectors $\mathbf{h}$ and $\mathbf{c}$ and supposing that the ith entry in $\mathbf{h}$ is nonzero, assuming $i \geq 1$, we obtain

$$c_i = h_i - \mathsf{g}(e^{\beta u(r_i)}(h_i + 1)) = h_i \left(1 - \frac{\mathsf{g}(e^{\beta u(r_i)}(h_i + 1))}{h_i}\right),$$

and therefore, if $h_j = \langle \mathbf{e}_j, \mathbf{h} \rangle = \|\mathbf{h}\|_\infty > 1$ and so $j \geq 1$ by the lower uniform bound $\mathbf{h} \geq -\mathbf{1}$, then

$$c_j = \|\mathbf{h}\|_\infty \left(1 - \frac{\mathsf{g}(e^{\beta u(r_j)}(\|\mathbf{h}\|_\infty + 1))}{\|\mathbf{h}\|_\infty}\right),$$

where $\|\cdot\|_\infty$ is the usual maximum norm of a vector. Hence, we may assume by choosing a subsequence if necessary that if $\mathcal{C}$ has a discrete vapor spinodal, then for some fixed, nonzero $j \in \{1, 2, \ldots, n\}$ there results

$$\frac{\|\mathbf{c}\|_\infty}{\|\mathbf{h}\|_\infty} \geq \frac{|c_j|}{\|\mathbf{h}\|_\infty} = \left|1 - \frac{\mathsf{g}(e^{\beta u(r_j)}(\|\mathbf{h}\|_\infty + 1))}{\|\mathbf{h}\|_\infty}\right|,$$

again provided $\|\mathbf{h}\|_\infty > 1$.

Thus, if $(\mathbf{h}_k, \mathbf{c}_k)$ is a sequence of solutions of (4.1)–(4.2) and $\|\mathbf{h}_k\| \to \infty$ as $k \to \infty$ in any norm, then $\|\mathbf{h}_k\|_\infty \to \infty$ as all finite-dimensional norms are equivalent. Since $\lim_{x \to \infty} \mathsf{g}(x)/x = 0$ it is clear that $\|\mathbf{c}_k\|_\infty / \|\mathbf{h}_k\|_\infty \to 1$ as $k \to \infty$ as claimed.

For the last part, suppose, without loss of any generality, that there is an $M > 0$ such that $\|\mathbf{h}_k\|_\infty \leq M$; then (4.3) shows that the jth component of $\mathbf{c}_k$, $|\langle \mathbf{e}_j, \mathbf{c}_k \rangle|$ for $j \geq 1$, is bounded above by

$$|\langle \mathbf{e}_j, \mathbf{c}_k \rangle| \leq M + \max_{-1 \leq x \leq M} g((x+1)e^{\beta \max_{j \geq 1}(u(r_j))}) < \infty, \tag{4.4}$$

which is potentially very large in practice but finite nevertheless.

Thus, the only way in which $\|\mathbf{c}_k\|$ can diverge is if $c_k := \langle \mathbf{e}_0, \mathbf{c}_k \rangle$ diverges as $k \to \infty$. From (4.1) there results

$$\langle \mathbf{e}_0, \mathbf{h}_k \rangle = c_k + \rho_k \langle \mathbf{e}_0, B(\mathbf{h}_k, \mathbf{c}_k) \rangle$$

so that

$$|c_k| \leq |\langle \mathbf{e}_0, \mathbf{h}_k \rangle| + \rho_{\max} |\langle \mathbf{e}_0, B(\mathbf{h}_k, \mathbf{c}_k) \rangle| \leq |-1| + \rho_{\max} |\langle \mathbf{h}_k, B(\mathbf{c}_k, \mathbf{e}_0) \rangle|.$$

Writing $\mathbf{c}_k = c_k \mathbf{e}_0 + \mathbf{c}_k^\perp$, where $\langle \mathbf{e}_0, \mathbf{c}_k^\perp \rangle \equiv 0$, we obtain

$$|c_k| \leq 1 + \rho_{\max} |\langle \mathbf{h}_k, B(c_k \mathbf{e}_0 + \mathbf{c}_k^\perp, \mathbf{e}_0) \rangle| \leq 1 + \rho_{\max} |\langle \mathbf{h}_k, B(\mathbf{c}_k^\perp, \mathbf{e}_0) \rangle|.$$

As a result, we finally obtain a bound on $|c_k|$ because of the existence of the pointwise upper bound (4.4) on $\mathbf{c}_k^\perp$, and so the final claim holds. ∎

We can now prove the following.

THEOREM 2. *Suppose that* G1–G3 *are satisfied by G, that $B = B_n$, and that the resulting equation* (3.8) *has a solution branch $\mathcal{C}$ with a discrete vapor spinodal. Take any sequence of solutions $(\mathbf{h}_k, \boldsymbol{c}_k)$ of* (4.1)–(4.2) *with density values ρ_k corresponding to solutions from $\mathcal{C}$ such that $\|\mathbf{h}_k\| \to \infty$ and $(\mathbf{h}_k)$ does not* localize at the cut-off *in the sense that*

$$\liminf_{k\to\infty} \frac{|\langle \mathbf{e}_j, \mathbf{h}_k\rangle|}{\|\mathbf{h}_k\|} > 0 \qquad \text{for some } j \in \{1,\dots,n-1\}.$$

Assuming also that $\langle \mathbf{e}_0, \mathbf{c}_k\rangle$ is a bounded sequence, if $\rho_k \to \rho_{\rm sp}$ as $k \to \infty$, then $\rho_{\rm sp} = 0$.

Proof. Let us begin by reformulating (4.1)–(4.2) by writing $\mathbf{c} = c_0\mathbf{e}_0 + \mathbf{c}^\perp$ and $\mathbf{h} = h_0\mathbf{e}_0 + \mathbf{h}^\perp$, where $\mathbf{c}^\perp, \mathbf{h}^\perp \in \text{span}\{\mathbf{e}_0\}^\perp$. Then (4.1) becomes

$$c_0\mathbf{e}_0 + \mathbf{c}^\perp = h_0\mathbf{e}_0 + \mathbf{h}^\perp + \rho B(c_0\mathbf{e}_0 + \mathbf{c}^\perp, h_0\mathbf{e}_0 + \mathbf{h}^\perp),$$

and projecting this onto $\text{span}\{\mathbf{e}_0\}$ gives

$$\begin{aligned}
c_0 &= h_0 - \rho\left\langle \mathbf{e}_0, B(c_0\mathbf{e}_0 + \mathbf{c}^\perp, h_0\mathbf{e}_0 + \mathbf{h}^\perp)\right\rangle \\
&= h_0 - \rho\left\langle B(\mathbf{e}_0, c_0\mathbf{e}_0 + \mathbf{c}^\perp), h_0\mathbf{e}_0 + \mathbf{h}^\perp\right\rangle \quad \text{(using B1 and B4)} \\
&= h_0 - \rho\left\langle B(\mathbf{e}_0, \mathbf{c}^\perp), h_0\mathbf{e}_0 + \mathbf{h}^\perp\right\rangle \\
&= h_0 - \rho\left\langle \mathbf{c}^\perp, B(\mathbf{e}_0, h_0\mathbf{e}_0 + \mathbf{h}^\perp)\right\rangle \quad (\text{since } B_n(\mathbf{e}_0, \mathbf{e}_0) = \mathbf{0}) \\
&= h_0 - \rho\left\langle \mathbf{c}^\perp, B(\mathbf{e}_0, \mathbf{h}^\perp)\right\rangle = h_0 - \rho\left\langle \mathbf{e}_0, B(\mathbf{c}^\perp, \mathbf{h}^\perp)\right\rangle.
\end{aligned}$$

However, from (4.2), $h_0 = -1$ as $(e^{-\beta\mathbf{U}})_0$ is interpreted as zero, whence

$$c_0 = -1 - \rho\left\langle \mathbf{e}_0, B(\mathbf{c}^\perp, \mathbf{h}^\perp)\right\rangle,$$

which defines a bilinear functional of $\mathbf{c}^\perp$ and $\mathbf{h}^\perp$ that depends affinely on ρ.

Now (4.1) can be projected onto $\text{span}\{\mathbf{e}_0\}^\perp$ with projector Π to yield

$$\mathbf{h}^\perp = \mathbf{c}^\perp + \rho\Pi B(c_0(\rho, \mathbf{c}^\perp, \mathbf{h}^\perp)\mathbf{e}_0 + \mathbf{c}^\perp, -\mathbf{e}_0 + \mathbf{h}^\perp), \tag{4.5}$$

$$\mathbf{h}^\perp = -\mathbf{1}^\perp + e^{-\beta\mathbf{U}^\perp} G(\mathbf{h}^\perp - \mathbf{c}^\perp), \tag{4.6}$$

where the advantage of this formulation is that $e^{-\beta\mathbf{U}^\perp}$ is strictly positive for any intermolecular potential, thus removing the problematic singularity at $r = 0$. Here, we are using a superscript $\perp$, as in $\mathbf{v}^\perp$, to denote the projection $\Pi(\mathbf{v})$. As a result, the singularity in (4.6) has been removed and (4.6) is now equivalent to

$$\mathbf{c}^\perp = \mathbf{h}^\perp - \mathbf{g}(e^{\beta\mathbf{U}^\perp}(\mathbf{h}^\perp + \mathbf{1}^\perp)). \tag{4.7}$$

Returning to the sequence of solutions from $\mathcal{C}$, define new sequences

$$P_k := \mathbf{h}_k^\perp/\|\mathbf{h}_k\| \quad \text{and} \quad Q_k := \mathbf{c}_k^\perp/\|\mathbf{h}_k\|,$$

as defined in the statement of the theorem; then

$$\frac{P_k - Q_k}{\|\mathbf{h}_k\|} = \rho_k \Pi B \left(\frac{\langle \mathbf{e}_0, \mathbf{c}_k \rangle \, \mathbf{e}_0}{\|\mathbf{h_k}\|} + Q_k, -\frac{\mathbf{e}_0}{\|\mathbf{h}_k\|} + P_k \right),$$

and

$$Q_k = P_k - \frac{\mathbf{g}(e^{\beta \mathbf{U}^\perp}(\mathbf{h}_k^\perp + \mathbf{1}^\perp))}{\|\mathbf{h}_k\|}. \tag{4.8}$$

Using standard compactness properties, one can find P' of unit norm such that $P_k \to P'$, and therefore $Q_k \to P'$ by (4.8) using the sublinearity of $\mathbf{g}$. As a result, we find that

$$\rho_k \Pi B \left(\frac{\langle \mathbf{e}_0, \mathbf{c}_k \rangle}{\|\mathbf{h_k}\|} + P', P' \right) \to 0$$

as $k \to \infty$.

By hypothesis we can find a $\rho_{\mathrm{sp}} \geq 0$ such that by extracting a further subsequence if necessary $\rho_{\mathrm{sp}} \Pi B \, (P', P') = \mathbf{0}$. If $\rho_{\mathrm{sp}} > 0$ then $\Pi B \, (P', P') = \mathbf{0}$ follows and so $B \, (P', P') = \alpha \mathbf{e}_0$. Recalling that $B = B_n$ in the statement of the theorem, $H^* (HP')^2 = \alpha \mathbf{e}_0$ whence $\alpha = 0$ by the fact that $H \mathbf{e}_0 = \mathbf{0}$. Hence $(HP')^2 = \alpha \mathbf{e}_0$ for some $\alpha \in \mathbb{R}$, so that $HP' = \sqrt{\alpha} \mathbf{e}_0$ giving $\alpha = 0$ as H is self-adjoint, so that finally $P' \in \mathrm{span}\{\mathbf{e}_0, \mathbf{e}_n\}$. By construction of the sequence (P_k), it follows that $P' \in \mathrm{span}\{\mathbf{e}_n\}$ which states that $\mathbf{h}_k$ localizes at the cut-off, contradicting an assumption of the theorem. ∎

From Theorem 2 we have the following trichotomy in terms of discrete vapor spinodals when using the convolution form $B = B_n$ in (4.1)–(4.2). If $\boldsymbol{\mathcal{C}}$ is that discrete vapor spinodal, at least one of the following applies along a sequence $(\mathbf{h}_k, \mathbf{c}_k, \rho_k) \in \boldsymbol{\mathcal{C}}$:

T1. Density ρ_k heads to zero,

T2. $\langle \mathbf{e}_0, \mathbf{c}_k \rangle$ is unbounded, or

T3. $\mathbf{h}_k / \|\mathbf{h}_k\|$ (up to a subsequence) tends toward the localized vector $\mathbf{e}_n$.

Note that each of T1, T2, and T3 represents a different, nonphysical possibility, and both T1 and T3 have been observed in practice when G takes the HNC form, even though G1 does not apply in that context. On the other hand, we have not observed T2 in practice. It is an immediate corollary of T1 that (4.1)–(4.2) has a fold bifurcation in the sense of Definition 2 at some value of the density parameter, and so one should expect to observe a folded geometry of isothermal vapor solution branches at subcritical temperatures.

4.1. Qualitatively correct convolution forms. The T1–T3 trichotomy again raises the central question of the choice of convolution form B in (3.8). There are advantages in defining B by

$$B(\mathbf{u}, \mathbf{v}) = F^T (F\mathbf{u} \otimes F\mathbf{v}) \quad \text{such that } FF^T = I \tag{4.9}$$

for some linear transformation F for the following reason. Such a choice for B allows one to introduce a *qualitatively correct* discrete compressibility functional, χ_d^{-1}, say, for (4.1)–(4.2) (with any nonlinearity G) by setting

$$\chi_d^{-1} = 1 - \rho \, \langle \mathbf{e}_0, F\mathbf{c} \rangle \, .$$

By the term *qualitatively correct*, we mean that unlike (4.1)–(4.2) which is realized on setting $B = B_n$, using instead the convolution form B which is based on such

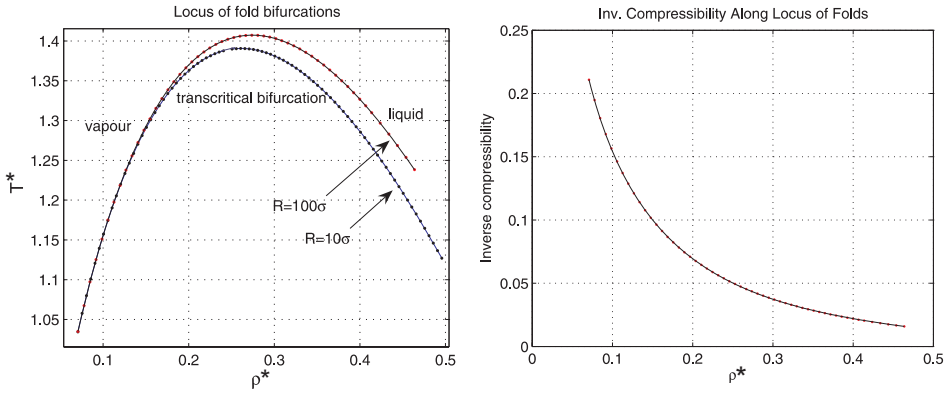

FIG. 5.1. *(Left) A comparison of two computed bifurcation loci for two values of R, namely,* 10σ *and* 100σ*. (Right) For the* $R = 100\sigma$ *case, inverse compressibility is evaluated along the liquid and vapor branches; note that this is never zero.*

a transformation F in (4.9) ensures that there is no solution of (4.1)–(4.2) that has zero inverse compressibility. This means that there is a version of Lemma 2.1 that holds when the convolution form B is based on (4.9), but Lemma 2.1 fails to hold when B_n is the chosen convolution form. We shall report the results of an analysis that results from the implemenation of a qualitatively correct convolution form in a separate publication.

5. Computations.

5.1. The LJ 6-12 potential. Throughout this section we use the Lennard–Jones potential and set $\sigma = 1, \epsilon = 1$, with the cut-off R chosen to be 100σ unless stated otherwise, and we have used a numerical mesh of $2^{13} + 1$ points.

1. Figure 5.1 (left) is a comparison of two codimension-two bifurcation loci in the (ρ, T)-plane that shows a significant discrepancy between the use of two choices of cut-off parameter R. The right-hand figure shows the values of inverse compressibility obtained along the loci from the left-hand curve for the $R = 100\sigma$ case. For *true spinodals*, which we gleaned from our previous analysis should not occur in the computations, this curve should be identically zero; clearly it is not.

One may notice that the curve in Figure 5.1 (left) lies slightly above that reported by others, such as [17, p. 833] and Figure 3 of [3]. The reasons for this are that the cut-off parameter R in the stated references is different from ours, and we have generally used a different number of points for our discretization than the cited articles. Our data may be slightly different also because we have computed the location of bifurcation points, rather than relying on the extrapolation of a numerical algorithm in order to estimate their location.

2. Figure 5.2 shows a computed unfolding of the transcritical bifurcation from the apex of Figure 5.1 (left), where nine different temperature values have been used to compute three subcritical isothermal solution branch pairs and six supercritical vapor isotherms. The appearance of several fold bifurcations can be seen on both liquid (high-density) and vapor (low-density) branches, and note the apparent existence of a locus of solutions of (3.6)–(3.7) with zero inverse compressibility.

3. Shown in Figure 5.3 (left) are the results of a computation undertaken with a *high* temperature at $\beta = 1$ and with $R = 120\sigma$; note the large number of fold bifurcations that seem to accumulate in the vicinity where inverse compressibility is

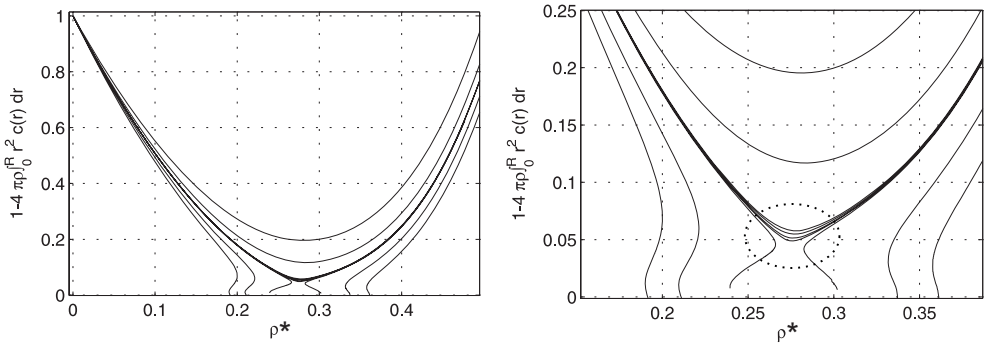

FIG. 5.2. *(Left) Inverse compressibility against density. (Right) Zoom of left-hand plot showing positive values of inverse compressibility at the fold points. Solutions with zero inverse compressibility are clearly seen but not* at *the fold bifurcations.*

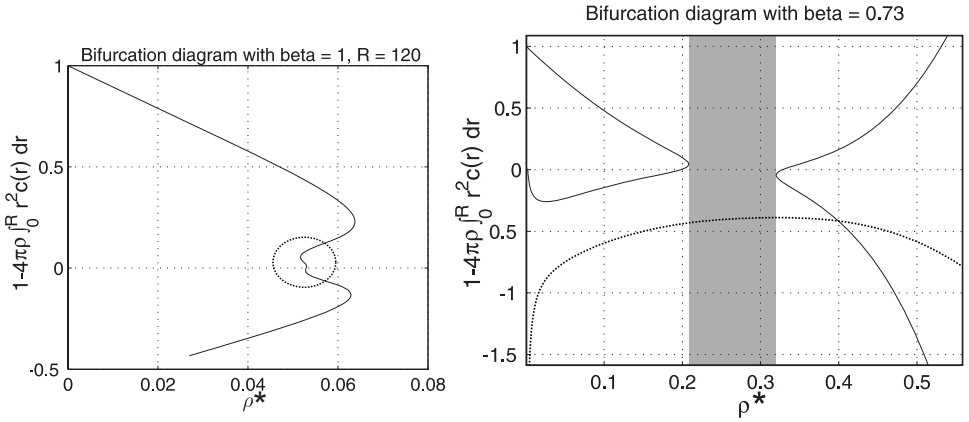

FIG. 5.3. *(Left) A solution branch with several bifurcations showing inverse compressibility against density with* $R = 120$ *and* $(1/T^* =)\beta = 1$. *(Right) Three solution branches and bifurcations with inverse compressibility plotted against density at* $R = 120$ *and* $\beta = 0.73$. *An apparent region (the shaded region) that contains no solutions is filled by a solution branch with negative compressibility.*

zero. In the right-hand figure we have located a branch of solutions at $\beta = 0.73$ that spans a shaded region where no solution is believed to exist, although this particular branch contains only solutions that have negative compressibility. Other branches of solutions have been found before within this region [21], but they were complex-valued and their presence was a simple consequence of the existence of fold bifurcations. We have not been able to locate any *real* solutions in this region with positive compressibility; that is not to say that none are there, but, unlike vapor isotherms, we have no systematic method for locating solutions in this region.

5.2. Comparison with the double Yukawa potential. For all of the following computations we used a numerical mesh with $2^{12} + 1$ points with the following double Yukawa (DY) intermolecular potential for various values of the cut-off R:

$$u_{DY}(r) = \frac{\epsilon}{r}\left(A_1 e^{-z_1(r-\sigma)} - A_2 e^{-z_2(r-\sigma)}\right),$$

where σ is particle diameter, and $A_1 = 1.6438\sigma$, $z_1 = 14.7\sigma^{-1}$, $A_2 = 2.03\sigma$, and $z_2 = 2.69\sigma^{-1}$ are the parameter values used in [8, 20]. This intermolecular potential

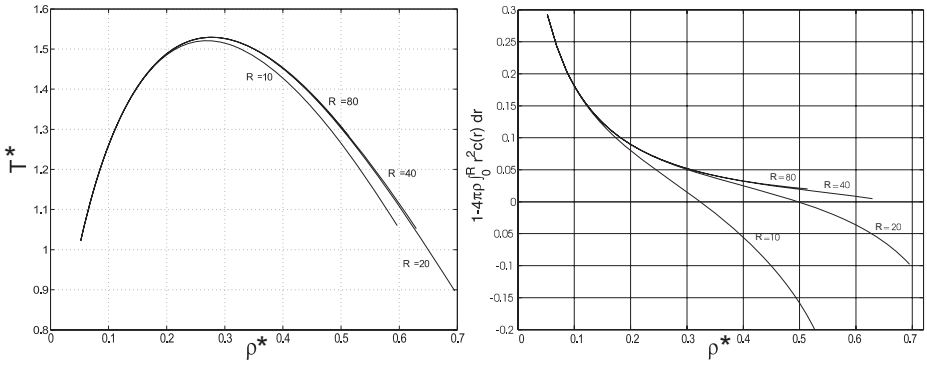

FIG. 5.4. *(Left) Locus of fold bifurcations for the DY potential with varied cut-offs and* 4096 *mesh points. (Right) Values of inverse compressibility along the locus for* $R = 10\sigma, \ldots, 80\sigma$.

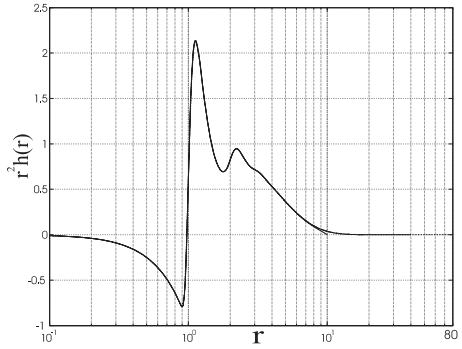

FIG. 5.5. *(Left) A plot of the low-density correlation function* $r^2h(r)$ *along the bifurcation locus from Figure* 5.4 *(left) at* $(\rho^*, T^*) = (0.085, 1.2)$ *for cut-off values* $R = 10\sigma, 20\sigma, 40\sigma$, *and* $R = 80\sigma$. *(Right) The high-density correlation function* $r^2h(r)$ *along the same bifurcation locus at* $(\rho^*, T^*) = (0.597, 1.06)$ *with* $R = 80\sigma$.

is commonly used as it has more rapid decay than LJ, with a repulsive soft core and attractive tail, which, it is believed, should lead to greater stability in computations. However, the property associated with the HNC closure of having L^1-divergence of the total correlation with L^2-boundedness at a spinodal is totally unaffected by the choice of potential and the decay rate of its tail.

1. Figure 5.4 is a repetition of Figure 5.1 for the DY potential for varying cut-offs: $R = 10\sigma, 20\sigma, 40\sigma$, and 80σ. The critical points at the apex of the locus in Figure 5.4 (left) are all close to $\rho_c = 0.27$ at $T_c = 1.52$. The curves corresponding to different cut-off points are in good agreement up to the apex but differ slightly beyond it; however, the values of inverse compressibility do vary somewhat with respect to the cut-off as shown in Figure 5.4 (right).

2. Figure 5.5 (left) illustrates a computed thermodynamic state with large compressibility that is located in the relatively low-density vapor Figure 5.4 (left), specifically at $(\rho^*, T^*) = (0.085, 1.2)$. Solutions have been computed with $R = 10\sigma, 20\sigma, 40\sigma$, and 80σ, and note that solutions at cut-offs higher than $R = 10\sigma$ are visually indistinguishable. A thermodynamic state from the high-density liquid region of Figure 5.4 (left) is shown in Figure 5.5 (right) for comparison.

Acknowledgments. Many thanks are due to Jim Henderson and Andrew Parry for their invaluable input to this work.

REFERENCES

[1] R. J. Baxter, *Percus-Yevick equation for hard spheres with surface adhesion*, J. Chem. Phys., 49 (1968), pp. 2770–2774.
[2] L. Belloni, *Inability of the hypernetted chain integral equation to exhibit a spinodal line*, J. Chem. Phys., 98 (1993), pp. 8080–8095.
[3] J. Brey and A. Santos, *Absence of criticality in the hypernetted chain equation for a truncated potential*, Mol. Phys., 57 (1986), pp. 149–160.
[4] J. J. Brey and A. Santos, *About the numerical solution of the Percus-Yevick equation in the critical region for nontruncated potentials*, J. Chem. Phys., 79 (1983), pp. 4652–4653.
[5] J. J. Brey, A. Santos, and F. Romero, *The critical region in the Percus-Yevick approximation. A numerical study for a Lennard-Jones potential*, J. Chem. Phys., 77 (1982), pp. 5058–5064.
[6] C. Caccamo, *Integral equation theory description of phase equilibria in classical fluids*, Phys. Rep., 274 (1996), pp. 1–105.
[7] P. T. Cummings and P. A. Monson, *Solution of the Ornstein-Zernike equation in the vicinity of the critical-point of a simple fluid*, J. Chem. Phys, 82 (1985), pp. 4303–4311.
[8] S. M. Foiles and N. W. Ashcroft, *Variational theory of phase separation in binary liquid mixtures*, J. Chem. Phys., 75 (1981), pp. 3594–3598.
[9] L. J. D. Frink and A. G. Salinger, *Rapid analysis of phase behavior with density functional theory.* II. *Capillary condensation in disordered porous media*, J. Chem. Phys., 118 (2003), pp. 7466–7476.
[10] L. J. D. Frink, A. G. Salinger, M. P. Sears, J. D. Weinhold, and A. L. Frischknecht, *Numerical challenges in the application of density functional theory to biology and nanotechnology*, J. Phys. Condens. Matter, 14 (2002), pp. 12167–12187.
[11] F. Gallerani, G. L. Vecchio, and L. Reatto, *Comment on the critical behavior in the Percus-Yevick equation*, Phys. Rev. A, 32 (1985), pp. 2526–2529.
[12] J. Hansen and I. Macdonald, *Theory of Simple Liquids*, Academic Press, London, 1976.
[13] J. R. Henderson and Z. A. Sabeur, *Liquid-state integral equations at high density: On the mathematical origin of infinite-range oscillatory solutions*, J. Chem. Phys., 97 (1992), pp. 6750–6758.
[14] H. B. Keller, *Numerical Solution of Bifurcation and Nonlinear Eigenvalue Problems*, P. Rabinowitz, ed., Academic Press, New York, 1977.
[15] C. T. Kelley and B. Montgomery-Pettitt, *A fast solver for the Ornstein–Zernike equations*, J. Comput. Phys., 197 (2004), pp. 491–501.
[16] R. J. F. Leote, R. Evans, D. C. Hoyle, and J. R. Henderson, *The decay of the pair correlation function in simple fluids: Long versus short-ranged potentials*, J. Phys. Condens. Matter, 6 (1994), pp. 9275–9294.
[17] E. Lomba and J. Lopez-Martin, *On the solutions of the hypernetted-chain equation inside the gas-liquid coexistence region*, J. Statist. Phys., 80 (1995), pp. 825–839.
[18] L. S. Ornstein and F. Zernike, *Accidental deviations of density and opalescence at the critical point of a single substance*, Proc. Akad. Sci. (Amsterdam), 17 (1914), pp. 793–806.
[19] J. K. Percus and G. J. Yevick, *Analysis of classical statistical mechanics by means of collective coordinates*, Phys. Rev. (2), 110 (1958), pp. 1–13.
[20] P. D. Poll and N. W. Ashcroft, *Critical behaviour of the hypernetted chain equation*, Phys. Rev. A, 35 (1987), pp. 5167–5173.
[21] G. Sarkisov and E. Lomba, *The gas-liquid phase-transition singularities in the framework of the liquid-state integral equation formalism*, Chem. Phys., 122 (2005), pp. 1–6.
[22] D. A. Tikhonov and G. N. Sarkisov, *Singularities of solution of the Ornstein–Zernike equation within a gas–liquid transition region*, Russian J. Phys. Chem., 74 (2000), pp. 470–476.
[23] J. M. J. van Leeuwen, J. Groeneveld, and J. D. Boer, *New method for the calculation of the pair correlation function*, Physica, 25 (1959), pp. 792–808.
[24] R. O. Watts, *Hypernetted-chain approximation applied to a modified Lennard-Jones fluid*, J. Chem. Phys., 50 (1969), pp. 1358–1365.
[25] E. Zeidler, *Nonlinear Functional Analysis and Its Applications* I: *Fixed Point Theorems*, Springer-Verlag, New York, 1986.